Applied Catalysis A, General 610 (2021) 117963

Contents lists available at ScienceDirect

Applied Catalysis A, General

journal homepage: www.elsevier.com/locate/apcata

Tuning Pt characteristics on Pt/C catalyst for aqueous-phase reforming of biomass-derived oxygenates to bio-H_2

A.K.K. Vikla [a,e], I. Simakova [b], Y. Demidova [b], E.G. Keim [c], L. Calvo [d], M.A. Gilarranz [d], Songbo He [a,f,*], K. Seshan [a]

[a] Faculty of Science and Technology, University of Twente, Drienerlolaan 5, 7522 NB, Enschede, The Netherlands
[b] Boreskov Institute of Catalysis, pr. Ak. Lavrentieva 5, 630090, Novosibirsk, Russia
[c] University of Twente, MESA+ NanoLab, Hallenweg 15, 7522 NH, Enschede, The Netherlands
[d] Department of Chemical Engineering, C/Francisco Tomás y Valiente 7, Universidad Autónoma de Madrid, 28049, Madrid, Spain
[e] Biomass Technology Group BV, Josink Esweg 34, 7545 PN, Enschede, The Netherlands
[f] Green Chemical Reaction Engineering, Engineering and Technology Institute Groningen, University of Groningen, Nijenborgh 4, 9747 AG, Groningen, The Netherlands

ARTICLE INFO

Keywords:
APR
Renewable
Ethylene glycol
Pt particle
Pt distribution

ABSTRACT

Pt/C catalysts with varied Pt sizes and distributions were investigated for aqueous-phase reforming (APR) of ethylene glycol (EG) to H_2. APR experiments were performed on a continuous-flow fixed bed reactor with a catalyst loading of 1 g and EG feeding of 120 mL h^{-1} at 225 °C and 35 bar for 7 h. The fresh and used Pt/C catalysts were characterized by XRF, BET, CO chemisorption, TEM, XTEM, and XPS. Catalyst preparation protocols changed Pt characteristics on Pt/C catalysts, leading to a distinguishable H_2 production. The rates for EG conversion and H_2 production increased linearly with mean Pt size (3–11 nm), while having a volcano relationship with the mean size of agglomerated Pt particles (17–30 nm). Pt with concentrated Pt particles on surface of Pt/C catalysts was more preferable for APR of EG than the homogeneously distributed in catalysts. Optimal performance was obtained over a Pt/C-PR catalyst, which was prepared by precipitation method, showing a superb turnover frequency of 248 mol_{H2} mol_{Pt}^{-1} min^{-1} for H_2 production from EG in APR. Besides, Pt/C catalysts also showed excellent stability. These results have shown the promise of Pt/C catalyst for APR of EG, which can be extended for bio-H_2 production *via* APR of biomass-derived oxygenates in waste streams.

1. Introduction

Renewable biomass-based feedstocks are hydrogen deficient and often require the use of external hydrogen to generate green fuels/blends that are compatible with the current fossil fuels [1,2]. Aqueous-phase reforming (APR) is a promising catalytic route to generate hydrogen from dilute aqueous streams containing organic molecules [3,4]. Byproduct and waste streams from food industries or biorefineries [5] often contain dissolved organics usually in the range of 5–20 wt.%. One typical example is the aqueous phase of pyrolysis oil which contains a variety of oxygenates such as acids, aldehydes, alcohols, sugars to name a few [2,4].

APR is a challenging process for a catalyst due to the drastic hydrothermal conditions (*e.g.*, 225–275 °C and 35–90 bar) used and complex feedstocks utilized, requiring an active and particularly stable catalyst [3]. Typically APR is carried out over supported metal catalysts, *e.g.,* Ni [6] and Pt [7] based catalysts. Critical issues for supports and active metals (*e.g.*, textural properties and phase changes, leaching, and sintering) [8] were often reported for APR catalysts. Recent developments have shown that Pt/C is a promising candidate for the APR of a variety of organic components [9–13].

Pt is, however, an expensive noble metal [14] and its loading on catalyst should be minimized for commercial application. This is generally achieved by altering Pt size (*e.g.* high dispersion [15]) and distribution (*e.g.*, egg-shell [16]) employing different supports. Several effective and controllable means, such as varying Pt loading [17], applying various preparation, calcination, and reduction protocols [18–20], have been reported.

Changing Pt size influences catalyst characteristics, which in turn, affects catalytic performance for APR. Lehnert et al. [21] studied APR of glycerol over Pt/Al_2O_3 catalyst and suggested that C-C cleavage in oxygenates (promoting the formation of C_1 species which can be steam

* Corresponding author at: Faculty of Science and Technology, University of Twente, Drienerlolaan 5, 7522 NB, Enschede, The Netherlands.
E-mail address: songbo.he@rug.nl (S. He).

https://doi.org/10.1016/j.apcata.2020.117963
Received 22 September 2020; Received in revised form 20 November 2020; Accepted 6 December 2020
Available online 11 December 2020

reformed to yield H_2 [2]) occurs preferentially on face Pt atoms, which increased with Pt particle size. Kirilin et al. observed a similar trend in turnover frequency (TOF) for different carbon-supported Pt catalysts for APR of xylitol [22]. However, Wawrzetz et al. [17] and Barbelli et al. [18] observed only a slightly increased TOF for Pt/Al_2O_3 catalysts with Pt size increase from 1.1 to 2.6 nm for APR of glycerol, relating it to the enhanced and simultaneous hydro-deoxygenation reactions consuming hydrogen. Ciftci et al. [23] studied Pt size domain of 1.2–4 nm and obtained an optimized performance for Pt size of *ca.* 2 nm for Pt/C catalysts for APR of glycerol. Chen et al. [24] screened an even wider Pt size range of 1.6–5.7 nm for Pt/Al_2O_3 catalyst for APR of low boiling point fraction of bio-oil and reported an optimized Pt size of 2.6 nm for H_2 production. These results are somehow contradictory. Nevertheless, it needs to be noted that in general, Pt size for the fresh catalysts was applied to correlate with catalyst performance.

As compared with the widely-investigated Pt size effect [24], the influence of distribution (uniform and egg-shell) of Pt with varied sizes on APR performance has not been reported yet to the best of our knowledge. In order to comprehensively study the effects of Pt size and also Pt distribution, we have applied different preparation protocols (*vide infra*) to make a variety of Pt catalysts with distinguishable Pt characteristics. Ethylene glycol (EG) was used as a model reactant to evaluate catalyst performance since it is a simple oxygenate with both carbon atoms connected to OH-groups. This allows to estimate the catalyst preference for C—C and C—O cleavage [25]. Besides, a carbon material was used as the catalyst support in this study, considering the variety of support materials (*e.g.*, Al_2O_3, SiO_2, ZrO_2, and TiO_2) that been extensively studied for supported Pt catalysts for APR of EG (Table 1). Pt/C catalysts show appreciable turnover frequency for H_2 production (TOF-H_2) compared with the state-of-the-art catalysts, namely Pt/AlO(OH) and Pt/SiO_2 (Table 1), both of which have stability problems. Therefore, the development of Pt/C catalyst is a valid argument and should aim to maximize TOF-H_2. Since a Sibunit carbon-supported Pt catalyst showed better H_2 productivity than other types of carbon materials supported Pt catalysts for APR of xylitol [22], it was used in this study to prepare the Pt/C catalysts. In total, four representative Pt/C catalysts with distinctive Pt characteristics such as small and agglomerated Pt particles, in a uniform fashion or with concentrated Pt particles on the surface in an egg-shell structure, are reported in this contribution. Moreover, the properties of the spent catalysts after 7-h APR of EG were correlated with the catalytic behavior.

2. Experimental

2.1. Materials

Sibunit carbon with a particle size of 100−200 μm was supplied by Boreskov Institute of Catalysis, Russia. H_2PtCl_6 was supplied by OAO Aurat, Russia. Pt-PVP colloid was prepared by a method published in Ref [33]. Analytical grade Na_2CO_3, formic acid, and ethylene glycol (EG, >99 %) were supplied by Sigma-Aldrich.

2.2. Catalyst preparation

Four Pt/C catalysts were prepared by variable methods, which are summarized in Table 2. Pt/C-IM and Pt/C-OX catalysts were prepared *via* incipient wetness impregnation with H_2PtCl_6 followed by drying in air overnight at 100 °C. Afterwards, the dried sample was reduced in H_2 at 320 °C for 6 h to produce the Pt/C-IM catalyst. Alternatively, the dried sample was further calcined at 420 °C for 6 h followed by a reduction in H_2 at 700 °C for 5 h to make the Pt/C-OX catalyst. Pt/C-PR catalyst was prepared by precipitation of H_2PtCl_6 with Na_2CO_3 followed by a

Table 1
TOF of Pt catalysts on various supports for bio-H_2 production from APR of EG in a continuous-flow fixed bed reactor.

Catalyst	Support supplier and preparation method	EG concentration (%)	Temperature (°C)	Pressure (bar)	TOF-H_2 (min^{-1})	Reference
Pt/Al_2O_3	γ-Al_2O_3, supplied by Argonide	1	225	29	0.08	Cortright et al. (2002) [4]
Pt/Al_2O_3	supplied by Condea, Catapal B	5	225	26	5.4	Huber et al. (2006) [25]
Pt/Al_2O_3	supplied by BASF, AL-3992	5	270	90	60	Koichumanova et al. (2013) [26]
Pt/SiO_2	supplied by Cabot, EH-5	5	210	22	75	Davda et al. (2003) [27]
Pt/AlO(OH)	produced by hydrothermal conversion of Al_2O_3 supplied by BASF (AL-3992) at 200 °C and 14 bar for 10 h	5	270	90	300	Koichumanova et al. (2013) [26]
Pt/ZnO	supplied by Alfa	10	225	29	1.6	Shabaker et al. (2003) [28]
Pt/CeO_2	–	10	250	46	0.7	Kim et al. (2013) [29]
Pt/CeO_2	supplied by Aldrich	10	225	29	1.2	Shabaker et al. (2003) [28]
Pt/ZrO_2	–	10	250	46	1.2	Kim et al. (2013) [29]
Pt/ZrO_2	supplied by Alfa	10	225	29	4.9	Shabaker et al. (2003) [28]
$Pt/Ce_xZr_{1-x}O_2$	$Ce_{0.15}Zr_{0.85}O_2$, prepared by Sol-Gel method	10	250	46	1.4	Kim et al. (2013) [29]
Pt/TiO_2	supplied by Degussa, P-25	10	225	29	11.1	Shabaker et al. (2003) [28]
Pt/Al_2O_3	supplied by Condea, Catapal B	10	225	29	6.7	Huber et al. (2006) [25]
Pt/Al_2O_3	supplied by Grace, Catapal B	10	225	29	9.4	Shabaker et al. (2003) [30]
Pt/α-Al_2O_3	α-Al_2O_3, produced by heating AlO(OH) at 1050 °C	10	225	29	25.2	Liu et al. (2011) [31]
Pt/δ-Al_2O_3	δ-Al_2O_3, produced by heating AlO(OH) at 850 °C	10	225	29	24.1	Liu et al. (2011) [31]
Pt/γ-Al_2O_3	γ-Al_2O_3, produced by heating AlO(OH) at 550 °C	10	225	29	23.7	Liu et al. (2011) [31]
Pt/SiO_2	supplied by Cabot, EH-5	10	225	22	275	Davda et al. (2003) [27]
Pt/SiO_2-Al_2O_3	supplied by Grace, MS-25	10	225	29	4.6	Shabaker et al. (2003) [28]
Pt/C	activated carbon, supplied by Norit, SX 1G	10	225	29	7.5	Shabaker et al. (2003) [28]
Pt/C	ordered mesoporous carbon, prepared using SBA-15 as template and furfuryl alcohol as carbon precursor	10	250	46	103	Kim et al. (2012) [32]
Pt/C	Sibunit carbon, supplied by Boreskov Institute of Catalysis, Pt/C-PR catalyst was prepared by precipitation method	2.5	225	35	248	Current work

Table 2
Characterizations of the fresh and used Pt/C catalysts.

Catalyst	Prepareation method		Pt loading (wt.%)[a]	S_{BET}(m^2 g^{-1})[b]	Pt Dispersion (%)[c]	Pt size (nm)[c]	Agglomerated Pt particles (nm)[d]	Pt content (wt.%)[e]		Pt (contrated on surface)
								Grains (100–250 μm)	Powder (< 40 μm)	
Pt/C-IM	incipient wetness impregnation, drying, reduction at 320 °C	Fresh	1.2	368	31	2.7	–	1.27	1.12	no
		Used	1.2	343	13	8.8	17	–	–	
Pt/C-OX	incipient wetness impregnation, drying, calcination at 420 °C, reduction at 700 °C	Fresh	1.4	340	29	2.9	–	1.27	1.28	no
		Used	1.2	326	34	3.4	–	–	–	
Pt/C-PR	precipitation with Na_2CO_3, reduction with HCOOH, drying, reduction at 700 °C	Fresh	0.8	372	22	4.2	11	2.67	1.74	+
		Used	0.7	343	11	10.7	21	–	–	
Pt/C-CL	wet impregnation with Pt-PVP colloid, drying, treated in HCW at 225 °C and 35 bar	Fresh	0.7	296	30	2.8	24	10.5	2.04	++
		Used	0.8	292	21	5.4	30	–	–	

By [a]XRF, [b]BET, [c]CO chemisorption, [d]XTEM and [e]XPS.
+ and ++ indicate a relative level for the concentration of Pt particles on surface.

reduction in formic acid. After drying in air, the dried sample was reduced in H_2 at 700 °C for 5 h. Pt/C-CL catalyst was prepared using a Pt-PVP colloid *via* wet impregnation. After drying in air, the sample was loaded to the APR reactor (*vide infra*) and treated in a hot compressed water stream (HCW, 2 mL/min) at 225 °C and 35 bar for 1 h, in order to remove PVP from the catalyst [20]. Afterwards, the sample was unloaded from the reactor and dried in air.

2.3. Catalyst characterization

Pt loading was semi-quantitatively analyzed by wavelength dispersive X-ray fluorescence (WDXRF) spectroscopy on S8 Tiger (Bruker) with the powder pellet method. An undiluted sample (*ca.* 0.5 g) was milled and loaded in a 29-mm die. Specific surface area (S_{BET}) was determined from N_2 physisorption measurement at -19,615 °C on Tristar 3000 (Micromeritics) according to the Brunauer-Emmett-Teller (BET) method [34]. Pt surface area and dispersion were determined by pulse CO chemisorption on ChemiSorb 2750 (Micromeritics). The catalyst was pretreated in He at 200 °C (5 °C min^{-1}) for 1 h, followed by pulse chemisorption of CO at room temperature. Pt dispersion was calculated by assuming that the adsorbed CO to Pt ratio is 1 [35]. Pt size was measured by high-resolution transmission electron microscopy (TEM) using a CM300ST-FEG (Philips) operated at 300 kV acceleration voltage. The catalyst was ultrasonicated in ethanol, followed by deposition on a carbon-coated copper grid. Approximately 250 particles across 10 spots were counted. The same transmission electron microscope was also used to record TEM images in cross-section (XTEM) images of catalyst grains to measure the size of agglomerated Pt particles. The catalyst particles were embedded in a resin (the details are shown in Supplementary Information, SI), which allows the observation in cross-section in order to locate the Pt nano-particles concentrated on the catalyst surface. Approximately 200 Pt particles for the Pt/C-PR and Pt/C-CL catalysts, and 50 Pt particles for the Pt/C-IM catalyst were counted for analyzing the mean size of the agglomerated Pt particles. Pt content on the catalyst surface was analyzed by X-ray photoelectron spectroscopy (XPS) in a Quantera Scanning X-ray Microprobe (PHI) equipped with an AlKα monochromatic X-ray source (1486.6 eV). The catalysts with two different particle sizes of 100–250 μm (for grains as-prepared) and 20−40 μm (for powder after grinding) were analyzed.

2.4. Catalyst testing

Aqueous-phase reforming of ethylene glycol solution (2.5 wt.% in water, feeding rate of 2 mL min^{-1}) over the Pt/C catalysts (loading of 1 g) was carried out on a bench-scale continuous-flow fixed bed reactor setup (Fig. 1) at 225 °C and 35 bar for a time on stream (TOS) of 7 h. The details of the experimental setup and procedure, and of the product analyses are given in SI. Catalyst performance was defined and calculated by using Eqs. 1–8.

$$\text{Conversion of EG } (\%) = \left(1 - \frac{\text{mol of EG in product}}{\text{mol of EG in feed}}\right) \times 100 \quad (1)$$

$$\text{Carbon yield of product } (\%) = \frac{\text{mol of carbon in liquid or gaseous product}}{\text{mol of carbon in in feed}} \times 100 \quad (2)$$

$$\text{Yield of } H_2\ (\%) = \frac{\text{mol } H_2 \text{ produced}}{\text{mol carbon converted}} \times \frac{1}{RR} \times X\ (\text{conversion}) \times 100 \quad (3)$$

$$\text{EG conversion rate } \left(\mu mol_{EG}\ A_{Pt}^{-1}\ min^{-1}\right) = \frac{\mu\text{mol of EG converted}}{\text{surface area of Pt} \times \text{TOS of 30 min}} \quad (4)$$

$$H_2 \text{ production rate } \left(\mu mol_{H_2}\ A_{Pt}^{-1}\ min^{-1}\right) = \frac{\mu\text{mol of } H_2 \text{ produced}}{\text{surface area of Pt} \times \text{TOS of 30 min}} \quad (5)$$

$$\text{TOF for } H_2 \text{ production } \left(mol_{H_2}\ mol_{Pt}^{-1}\ min^{-1}\right) = \frac{\text{mol of } H_2 \text{ produced}}{\text{mol of Pt} \times \text{TOS of 30 min}} \quad (6)$$

$$\text{Selectivity for carbon species} = \frac{\text{mol of carbon in liquid or gaseous product}}{\text{mol of carbon in in feed} * \text{conversion of EG}} \times 100 \quad (7)$$

$$\text{Selectivity for } H_2 = \frac{\text{mol } H_2 \text{ produced}}{\text{mol carbon converted}} \times \frac{1}{RR} \quad (8)$$

3. Results and discussions

3.1. Characterization of fresh catalysts

Various methods (Section 2.2 and Table 2) have been applied to prepare the four Pt/C catalysts with distinguishable Pt particle sizes and distributions (*viz.*, with concentrated Pt particles on the surface or in a homogeneous fashion). BET surface areas (Table 2) of fresh Pt/C-IM, Pt/C-OX, and Pt/C-PR catalysts (340 - 372 m^2 g^{-1}) are relatively close to

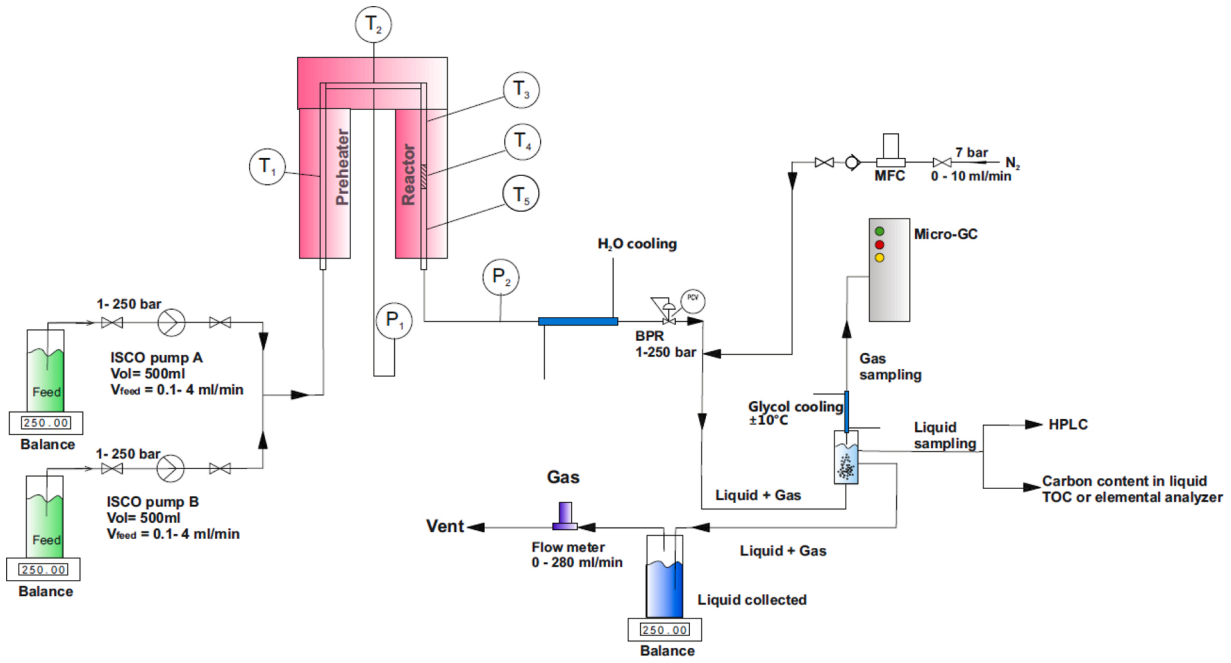

Fig. 1. Schematic representation of setup for APR of EG.

that of the Sibunit carbon support (350 $m^2\ g^{-1}$). However, a decreased S_{BET} was observed on the fresh Pt/C-CL catalyst (296 $m^2\ g^{-1}$), indicating that wet impregnation with the Pt-PVP colloid influenced textural property of the Sibunit carbon though a low amount of Pt (0.7 wt.%, Table 2) was loaded on the Pt/C-CL catalyst. This is most likely related to Pt concentrated on the catalyst surface (*vide infra*), due to the lower penetration of the Pt colloid into the pores of the support.

XPS analyses (Table 2, the corresponding spectra are shown in Figs. S1-S4) of the as-prepared catalyst grains (100–250 μm) and the after-ground powder (20−40 μm) show that the Pt concentration on the outer shell is higher than in the inner core of the Pt/C-IM, Pt/C-PR, and Pt/C-CL catalysts. Particularly, the difference is extremely large for the latter two catalysts, showing that the Pt concentrations on the outer surface are approximately 53 % (Pt/C-PR catalyst) and 4 times (Pt/C-CL catalyst) higher than the inner ones. Comparatively, the Pt/C-OX catalyst, which was prepared by incipient wetness impregnation followed by calcination and reduction at high temperatures, shows a similar Pt concentration on the outer surface and in the inner core. This might indicate that Pt was relatively homogeneously distributed in the Pt/C-OX catalyst, while Pt was more concentrated on the surface of the Pt/C-PR and Pt/C-CL catalysts.

The speculation about concentrated Pt particles on the surface of the Pt/C-PR and Pt/C-CL catalysts is further confirmed by XTEM images of the catalysts as prepared, showing that the Pt particles are more visible on the catalyst grain edge than in the core (Fig. 2C and D). XTEM images of the grain cores (Fig. 2C and D, right) display the fairly even distributed small Pt particles (< 3 nm). Comparatively, more concentrated small Pt particles are observed on the grain edges (Fig. 2C and D, left). Besides, agglomerated Pt particles with mean sizes of 11 nm and 24 nm (Table 2) are also present on the grain edges (with an approximate depth of 500 nm) of Pt/C-PR and Pt/C-CL catalysts. These are totally different from the XTEM images of the Pt/C-OX catalyst (Fig. 2B), showing that small Pt particles were evenly distributed on both the edge and in the core. No agglomerated Pt particles are observed on the Pt/C-OX catalyst, confirming the homogeneity of the Pt particles on the catalyst.

The uniformly distributed Pt with a small particle size on the Pt/C-OX catalyst is also evidenced by the sharp Pt particle distribution of 1–3 nm (Fig. 3B) analyzed by TEM. The broader Pt particle size distributions for the Pt/C-PR (1–9 nm, Fig. 3C) and Pt/C-CL (1–6 nm, Fig. 3D) catalysts are most likely related to the larger Pt particles present in the outer shell of the Pt/C-PR and Pt/C-CL catalysts.

The mean Pt particle sizes analyzed by CO chemisorption (Table 2) and TEM (Table S2) indicate that the Pt/C-IM and Pt/C-OX catalysts have smaller Pt particle sizes compared with the Pt/C-PR and Pt/C-CL catalysts. It needs to be noted that the Pt particle sizes estimated from CO chemisorption and TEM differ significantly, considering that only limited particles were counted from the TEM images (*e.g.*, 200–400, Fig. 3) and CO chemisorption might over-estimate (Pt−CO stoichiometry) Pt surface area. Nevertheless, the above trends in the Pt particle sizes for the four Pt/C catalysts are similar according to these two analyses.

As shown above, the catalysts prepared by the incipient wetness impregnation method, *viz* Pt/C-IM, and Pt/C-OX catalysts, have uniformly distributed small-size Pt particles. This is different from the catalysts prepared by precipitation (*viz.*, Pt/C-PR catalyst) and wet impregnation with Pt colloid (*viz.*, Pt/C-CL catalyst), which have small and also large Pt particles concentrated on the outer shell of the catalyst grains. According to the semi-quantified Pt content (by XPS, Table 2) and the visual Pt distribution (by XTEM, Fig. 2) on the catalyst edge and in the catalyst core for the four Pt/C catalysts investigated, the Pt/C-CL catalyst has the highest degree of Pt concentration on the catalyst surface, followed by the Pt/C-PR and Pt/C-IM catalysts (Table 2). Pt on the Pt/C-OX catalyst is distributed in a more homogeneous fashion as compared with that on the Pt/C-IM catalyst, indicating that high-temperature calcination and reduction enhanced the homogeneity of Pt on the Pt/C catalysts [36].

3.2. Performance of Pt/C catalysts in APR of EG

Aqueous-phase reforming of ethylene glycol over the above four Pt/C catalysts were continuously performed on a fixed bed reactor at 225 °C and 35 bar for 7 h. Catalyst performance over TOS is shown in Fig.4A in terms of EG conversion. In general, the initial EG conversion is comparable (*e.g.*, 37.5–39.4 %) among the Pt/C catalysts investigated, except for the Pt/C-OX catalyst which shows a relatively lower EG conversion of 26.7 %. All the Pt/C catalysts exhibited excellent stability, evidenced by only a slight drop (*ca.* 4–5 %) in EG conversion after TOS of 3.5 h. Negligible deactivation occurred afterwards, indicating a steady state of

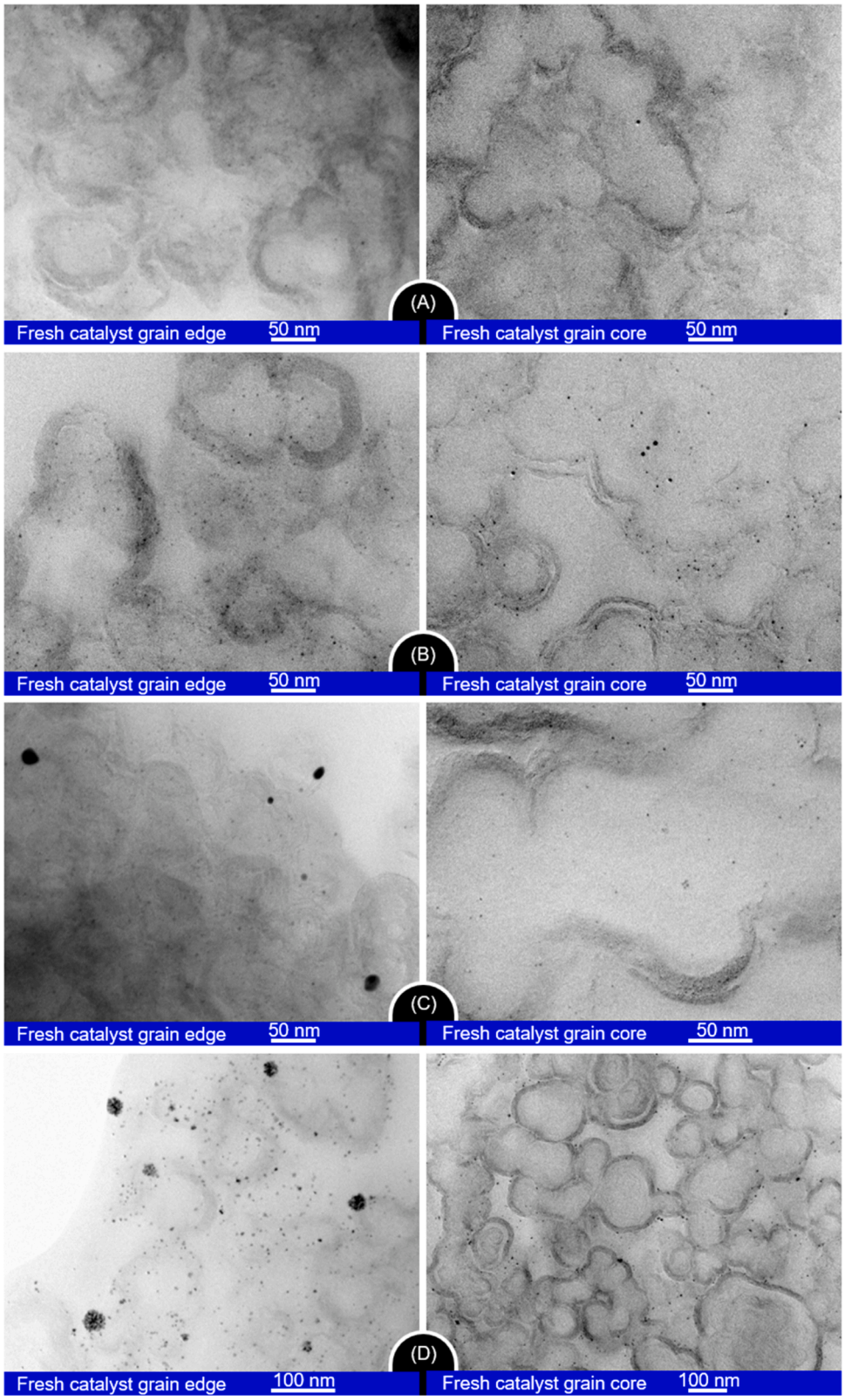

Fig. 2. XTEM images for grains edge (left) and core (right) of the fresh Pt/C-IM (A), Pt/C-OX (B), Pt/C-PR (C) and Pt/C-CL (D) catalysts.

the Pt/C catalysts for EG conversion. Accordingly, the products during TOS of 3.5–7 h were averaged to evaluate the representative products from APR of EG over the Pt/C catalysts.

The excellent total carbon balance closures (*e.g.*, 97–101 %) indicate negligible coke formation during APR of EG over the Pt/C catalysts. The selectivity's to various products are shown in Table 3. The major carbon-related products are gases, which consist of CO, CO_2 and CH_4 (Fig. 4B). A very small amount of EG was converted to liquid phase products (Fig. 4C) such as methanol, ethanol, acetic acid, glycolaldehyde and larger polyol (*e.g.*, glycerol).

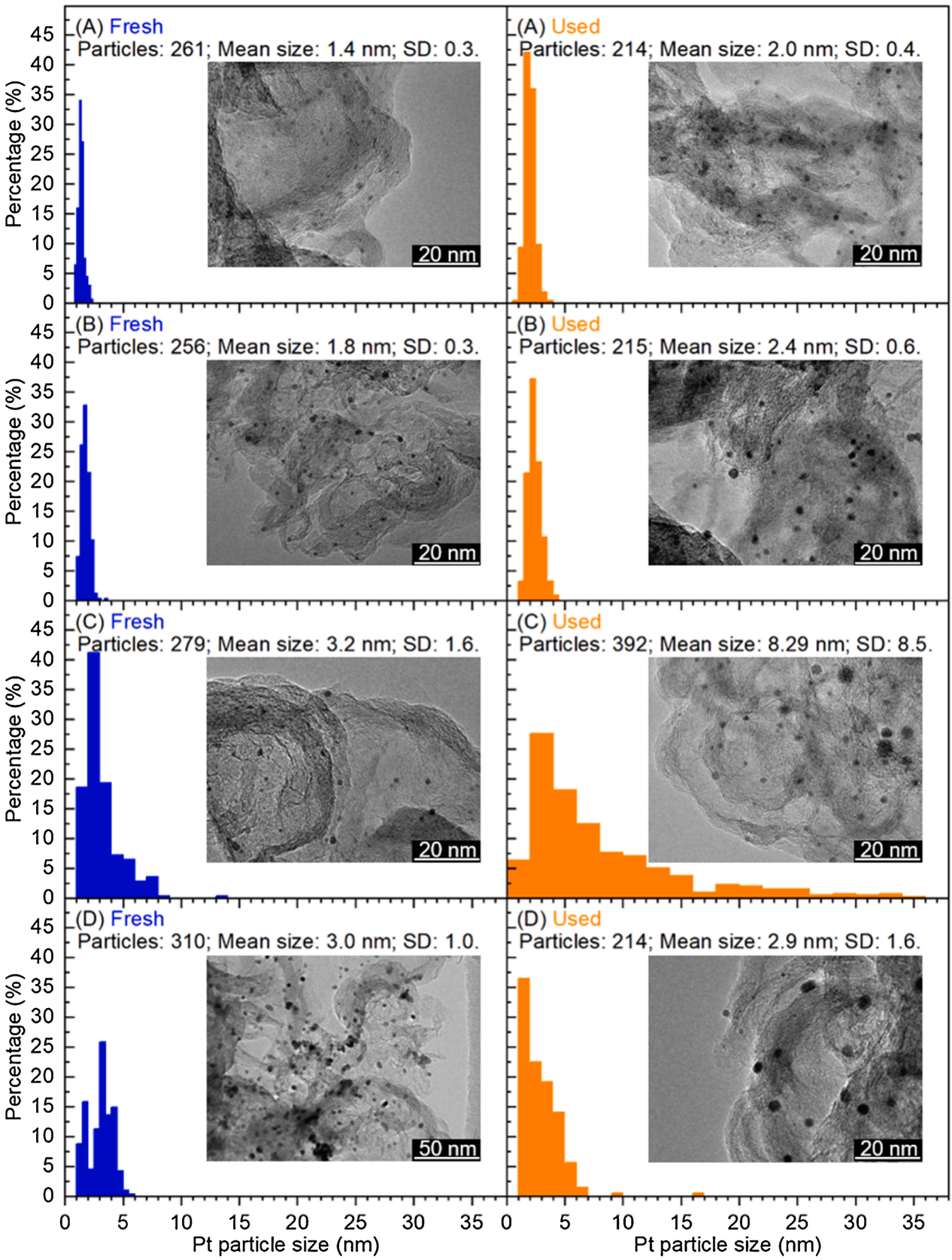

Fig. 3. TEM images and Pt particle size distributions for the fresh (left) and used (right) Pt/C-IM (A), Pt/C-OX (B), Pt/C-PR (C) and Pt/C-CL (D) catalysts.

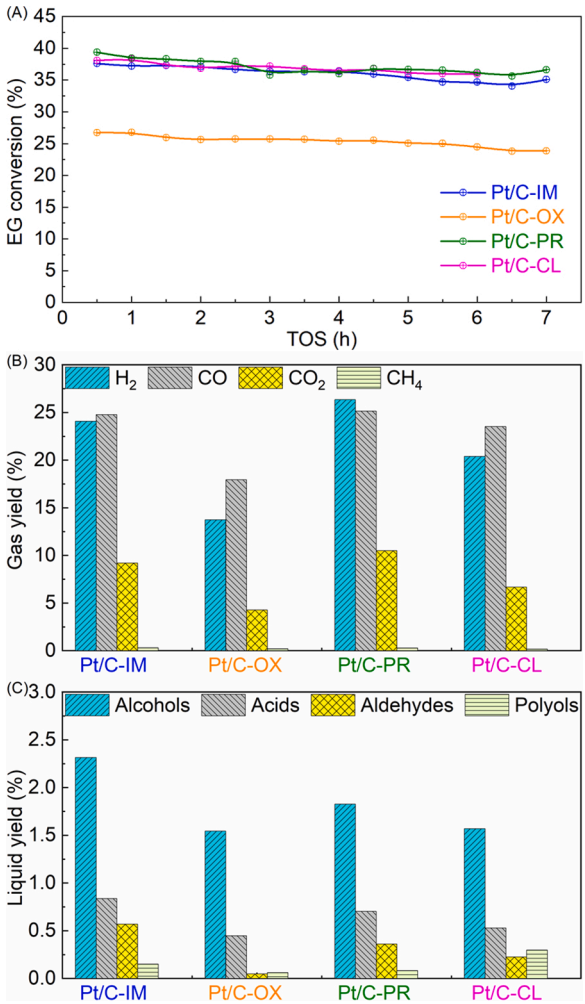

Fig. 4. EG conversion *versus* TOS (A), average yields of gaseous (B) and liquid (C) products during TOS of 4 - 6 h over Pt/C-IM, Pt/C-OX, Pt/C-PR and Pt/C-CL catalysts.

Table 3
Selectivity's for carbon specieces and H_2 over the four Pt/C catalysts.

	Pt/C-PR	Pt/C-CL	Pt/C-IM	Pt/C-OX
Glycerol	0.2	0.8	0.4	0.2
Formic Acid	0.2	0.2	0.1	0.1
Acetic Acid	0.3	0.2	0.0	0.0
Acetaldehyde	0.2	0.1	0.8	0.0
Methanol	4.3	4.0	6.5	5.4
Ethanol	0.3	0.3	0.1	0.1
Glycolaldehyde	0.7	0.5	0.8	0.1
Glycolic acid	1.7	1.1	2.2	1.4
CO	65.9	64.8	70.2	72.0
CO_2	24.4	18.4	26.0	17.1
CH_4	0.8	0.5	0.9	0.8
C_2	0.1	0.1	0.1	0.1
H_2	63.9	56.2	68.2	55.1

The yield of the most interesting product, *viz.*, H_2 (Fig. 4B), differs dramatically with the Pt/C catalysts. Pt/C-PR catalyst has the highest H_2 yield (26.4 %), followed by Pt/C-IM (24.1 %), Pt/C-CL (20.4 %) and Pt/C-OX (13.7 %) catalysts. This points to the different characteristics of active Pt sites on the four Pt/C catalysts.

3.3. Characterization of the used catalysts

As discussed above, the Pt/C catalysts evolved to the steady-state after a TOS of 3.5 h (Fig. 4A). To correlate the catalyst characteristics with the catalytic performance during the 3.5–7 h TOS period (Fig. 4B and C), the used Pt/C catalysts after continuous-flow APR of EG for 7 h were characterized. The four used Pt/C catalysts showed comparable BET areas (326 - 343 $m^2\ g^{-1}$, Table 2) with the fresh ones, indicating insignificant changes in catalyst pore structure after 7-h TOS. In addition, the Pt loadings on the fresh and used Pt/C catalysts (Table 2) are similar, showing a negligible loss of Pt under the severe APR reaction conditions.

However, Pt particle sizes are larger on the used Pt/C catalysts than on the fresh ones according to both CO chemisorption and TEM analyses (Tables 2 and S2, and Fig. 3). The growth of Pt particles during APR reactions was often observed on supported Pt catalysts, *e.g.*, Pt/C [13] and Pt/Al_2O_3 [8]. As a consequence, the Pt particle size distributions for the used Pt/C catalysts were broadened (Fig. 3), which is particularly significant for the Pt/C-PR catalyst (Fig. 3C). The mean Pt particle size on the Pt/C-PR catalyst was dramatically increased from 3.2 to 8.3 nm as measured by TEM (Table S2), and from 4.2 to 10.7 nm as measured by CO chemisorption (Table 2). Comparatively, the Pt/C-OX and Pt/C-CL catalysts show smaller changes on the Pt particle size. For the latter catalyst, the high-degree Pt concentration on catalyst surface with agglomerated Pt particles (Section 3.1) might have resistance to a further Pt agglomeration [37], which is reflected by the slightly increased Pt particle size (Table 2) from 24 nm for the fresh Pt/C-CL catalyst (Fig. 2D) to 30 nm for the used one (Fig. 5C). Besides, the preparation method for the Pt/C-CL catalyst also has influence on the stability, *e.g.*, by hydrothermal treatment to remove PVP and to stabilize the nanoparticles on the support [20]. Whereas for the Pt/C-OX catalyst, the stability of the Pt particle size might be related to the high-temperature calcination and the reduction enhancing Pt and C interaction [36]. As such, a further check of the presence of the agglomerated Pt particles on the used Pt/C-OX catalyst by XTEM was not carried out, considering that no agglomerated Pt particles presented on the fresh catalyst (Fig. 2B) as well.

XTEM images of the used Pt/C-PR catalyst (Fig. 5B) show larger Pt particles (*e.g.*, 20–40 nm) on the catalyst edge as compared with the fresh catalyst (Fig. 2C), resulting in a nearly doubled Pt particle size (Table 2). This is in good agreement with the change on mean Pt particle size (by TEM (Table S2) and CO chemisorption (Table 2)) on the Pt/C-PR catalyst after the APR reaction. Similarly, agglomerated Pt particles with a mean size of 17 nm (Table 2) were also formed on the used Pt/C-IM catalyst edge (Fig. 5A), in line with the increased mean Pt particle size from 2.7 nm (for the fresh catalyst, by CO chemisorption, Table 2) to 8.8 nm (for the used catalyst, Table 2). It needs to be noted here that no agglomerated Pt particles are observed in the core of the catalyst (Fig. 5-right), indicating the Pt agglomeration mainly took place on the surface of the Pt/C catalyst under APR conditions.

3.4. Discussion

It was demonstrated above that a stable catalytic performance in APR of EG in terms of EG conversion and H_2 production was obtained over Pt/C catalysts, which were prepared by a different method in order to alter Pt size and Pt distribution on a Sibunit carbon support. In this contribution, we have used the diluted solution to investigate the relationship between APR performance and catalyst characteristics. For such a diluted stream, the industrial implementation of APR should be further considered, *e.g.*, the economic feature related to the energy consumption for heating the H_2O.

To recall, the Pt/C catalysts prepared by a general method as incipient wetness impregnation (*viz.*, Pt/C-IM and Pt/C-OX catalysts), have evenly distributed Pt particles with small sizes. A high-temperature treatment, *e.g.* calcination followed by reduction, was applied to strengthen the interaction between Pt and carbon support. As a consequence, the Pt/C-OX catalyst showed much better stability on Pt size and Pt distribution under the severe APR conditions than the Pt/C-IM

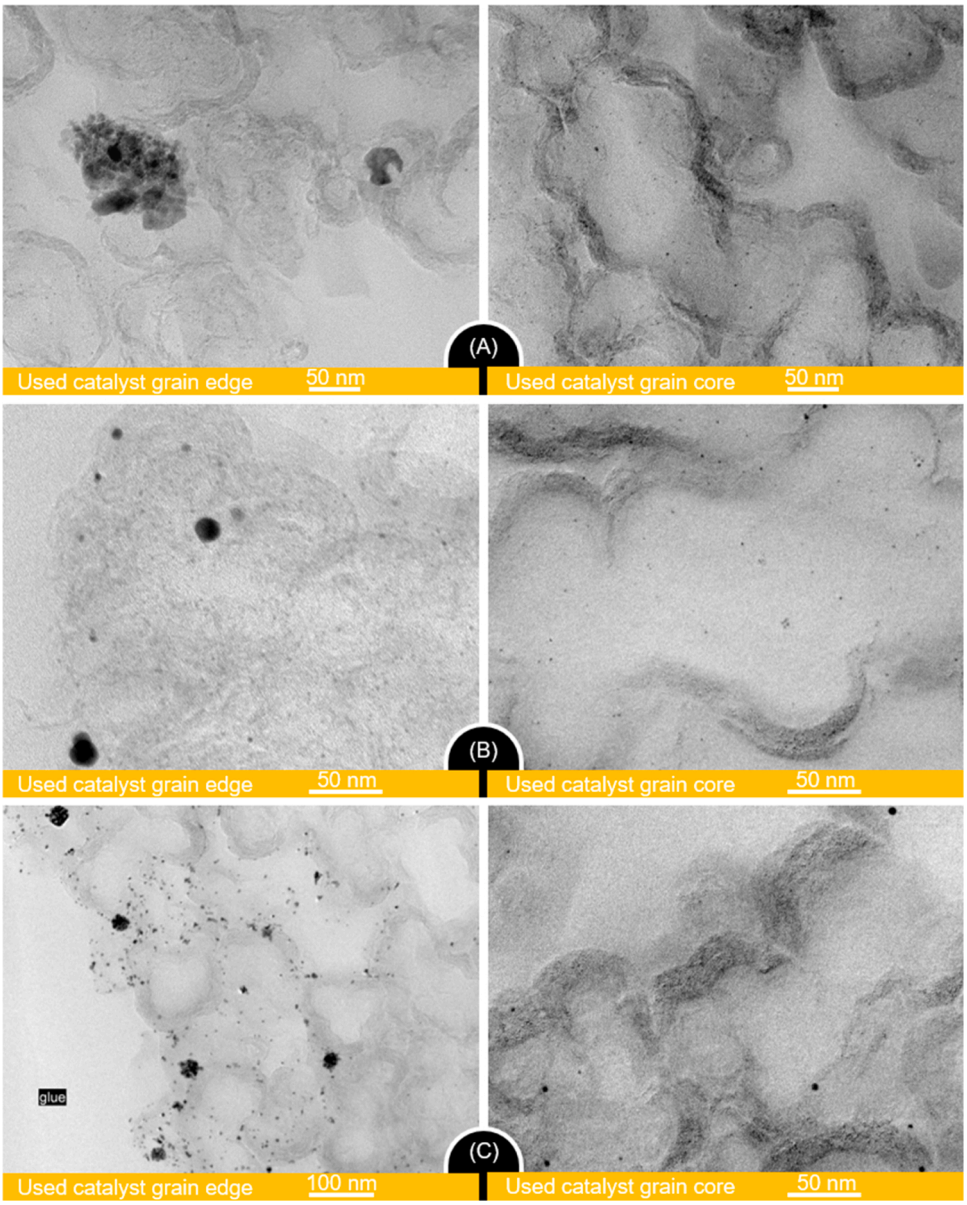

Fig. 5. XTEM images for grains edge (left) and core (right) of the used Pt/C-IM (A), Pt/C-PR (B) and Pt/C-CL (C) catalysts.

catalyst having agglomerated Pt particles on catalyst surface after 7-h APR of EG. Alternatively, the Pt/C catalysts prepared by precipitation method (Pt/C-PR catalyst) and a more novel method of impregnation of pre-prepared Pt colloid (Pt/C-CL catalyst) obtained small Pt particles, as well as agglomerated Pt particles concentrated on the catalyst grain edge. It seems that the inhomogeneous Pt distribution formed on the surface of Pt/C-PR and Pt/C-CL catalysts, and the degree of Pt concentration on the surface of the latter is higher than that of the former. Compared with the Pt/C-CL catalyst, the fresh Pt/C-PR catalyst has more amount of agglomerated Pt particles with a smaller size, resulting in a bigger mean Pt particle size (Table 2). However, these small Pt particles on the Pt/C-PR catalyst grew faster than those large Pt particles on the Pt/C-CL catalyst under the APR reaction conditions. As such, the mean Pt particle size for the Pt/C-PR catalyst increased remarkably, while only a slightly increased mean Pt particle size was observed for the Pt/C-CL catalyst.

Since all the Pt/C catalysts were prepared using the same Sibunit carbon support, any difference observed in the chemistry, *e.g.*, product distribution, over different Pt/C catalysts (Fig. 4) should be related to Pt characteristics, *e.g.*, Pt particle size and its distribution. In order to properly correlate the catalyst performance with the catalyst characteristics, the *in-situ* characterizations of the catalyst during APR is required, *e.g.*, by an *in-situ* attenuated total reflectance Fourier transform infrared (ATR-IR) technique [26]. However, this is very challenging for Pt/C catalysts, due to the fact that the refractive index of carbon and the internal reflection element (ZnSe) is too similar to obtain ATR-IR spectra for carbon-supported catalysts. The fresh catalyst might change greatly under APR conditions even after a short TOS [38], leading to an inappropriate relationship between initial catalyst performance with fresh catalyst characteristics. Considering that the Pt/C catalysts evolved to a relatively steady state after TOS of 3.5 h (Section 3.2), it might be assumed that Pt/C catalyst characteristics remain stable during TOS of 3.5–7 h. Therefore, the averaged EG conversion (Fig. 4A) and H_2 production (Fig. 4B) during TOS of 3.5–7 h, and the characteristics of Pt on the used Pt/C catalysts (Table 2) after TOS of 7 h were used to calculate reaction rates by using Eqs. 4 – 6. In addition, Pt can be taken as metallic Pt during the APR reactions, considering that the pre-reduction of the Pt/C catalysts was performed at temperatures higher than the reduction temperature of PtO_x for Sibunit carbon supported Pt catalysts (*e.g.*, T_{max} of 125 °C [22]). Even though there might be a very small fraction of PtO_x

species due to the partial oxidation during the storage and loading to the reactor [22], they would probably be reduced by the H_2 formed during APR at a reaction temperature of 225 °C. In order to study the effect of Pt size on catalyst performance, EG conversion and H_2 production rates based on the available Pt surface area ($\mu mol_{EG(or\ H2)}\ A_{Pt}^{-1}\ min^{-1}$) are shown in Fig. 6A. The mean Pt particle size (Fig. 6A) and the mean size for the agglomerated Pt particles (Fig. 6B) were analyzed by CO chemisorption and XTEM, separately.

It is interesting to observe that the rates for both EG conversion and H_2 production increased linearly with the increased Pt particle sizes. Comparatively, the sensitivity to Pt particle size for H_2 production rate is higher than for an EG conversion rate, as indicated by the slopes of the fitted lines in Fig. 6A. This result is consistent with that reported by Lehnert et al. [21], who also observed a higher H_2 production from APR of glycerol over Pt/Al_2O_3 catalysts with a bigger Pt particle size. This is most likely related to the enhanced C-C cleavage of oxygenates on more Pt surface forming H_2, in turn competing for C-O cleavage reaction yielding low hydrocarbons [2]. The extremely low yields of C_1 and C_2 hydrocarbons (Fig. 4B) also confirm this.

It needs to be highlighted here that the mean Pt particle sizes on the Pt/C catalysts in this study are quite big (*e.g.*, 3–11 nm in Fig. 6A), related to the presence of large Pt particles. The correlations between Pt particle size and the rates for EG conversion and H_2 production (Fig. 6-B) suggest that a mean size for agglomerated Pt particles of *ca.* 20.7 nm is the most suitable. There is a trade-off of the size of the agglomerated Pt particles for an optimal H_2 production rate over Pt/C catalysts, due to the fact that the number of exposed surface Pt atoms continues to decrease as the size of agglomerated Pt particles increases. As a consequence, the Pt/C-PR catalyst, which has a number of Pt particles with small size concentrated on the catalyst grain edge, has the highest TOF for H_2 production of 248 $mol_{H2}\ mol_{Pt}^{-1}\ min^{-1}$ (Fig. 7). Comparatively, the Pt/C-CL catalyst of which the level of Pt concentration on the surface is the highest has a much lower TOF-H_2 (100 $mol_{H2}\ mol_{Pt}^{-1}\ min^{-1}$, Fig. 7), due to the presence of Pt particles with a large size. For the Pt/C-IM catalyst, which has the Pt particles relatively homogeneously distributed both on the grain edge and in the core of the catalyst, has a much higher TOF-H_2 (78 $mol_{H2}\ mol_{Pt}^{-1}\ min^{-1}$, Fig. 7) than the Pt/C-OX catalyst (18 $mol_{H2}\ mol_{Pt}^{-1}\ min^{-1}$, Fig. 7). This is obviously related to the bigger mean Pt particle size for the Pt/C-IM catalyst compared with the Pt/C-OX catalyst.

Of great interest is that the highest TOF-H_2 (248 $mol_{H2}\ mol_{Pt}^{-1}\ min^{-1}$) obtained on the Pt/C-PR catalyst in this study is much higher than those reported Pt/C catalysts (Table 1) by Shabaker et al. (7.5 $mol_{H2}\ mol_{Pt}^{-1}\ min^{-1}$) [28] and Kim et al. (103 $mol_{H2}\ mol_{Pt}^{-1}\ min^{-1}$) [32], representing the best performance of Pt/C for APR of EG to bio-H_2. Furthermore, what is significant is that the TOF-H_2 of Pt/C-PR is close to the top two catalysts (*viz.*, Pt/AlO(OH) catalyst with a TOF of 300 $mol_{H2}\ mol_{Pt}^{-1}\ min^{-1}$ [26] and Pt/SiO_2 catalyst with a TOF of 275 $mol_{H2}\ mol_{Pt}^{-1}\ min^{-1}$ [27]) developed for APR of EG so far.

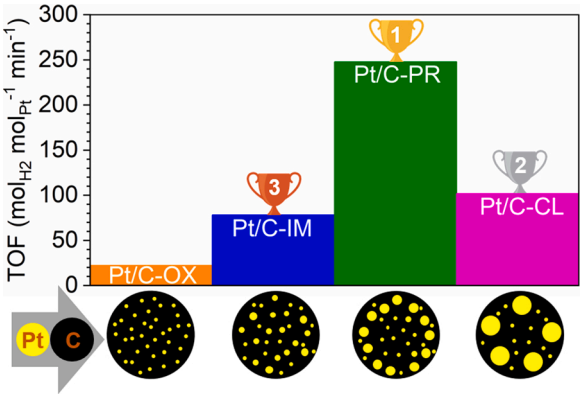

Fig. 7. Schematic representation of the used Pt/C catalysts and their TOFs for H_2 production.

Stability of Pt/SiO_2 catalyst, related to the leaching of silica under APR conditions, is a critical issue for a long-term practical application [39]. Pt/AlO(OH) catalyst might have a high tendency for coke formation during APR [40] due to the acidity of AlO(OH) support [41]. It has been demonstrated in this study that the Sibunit carbon is stable under APR conditions and coking on Pt/C catalyst is negligible during a continuous 7-h APR of EG (Section 3.2). Besides, using carbon as a carrier for supported Pt catalysts ensures that it is easy to harvest Pt for recycling after usage by burning [42]. Having a high intrinsic activity for hydrogen production and an excellent stability for long-term operation, Pt/C catalyst could definitely be an excellent catalyst for APR of oxygenates for bio-H_2 production.

Pt concentrated on the catalyst surface with small-size Pt particles on Pt/C catalyst is advantageous for APR of a small molecule (*viz.*, EG), which might also be significant for larger oxygenates. Further

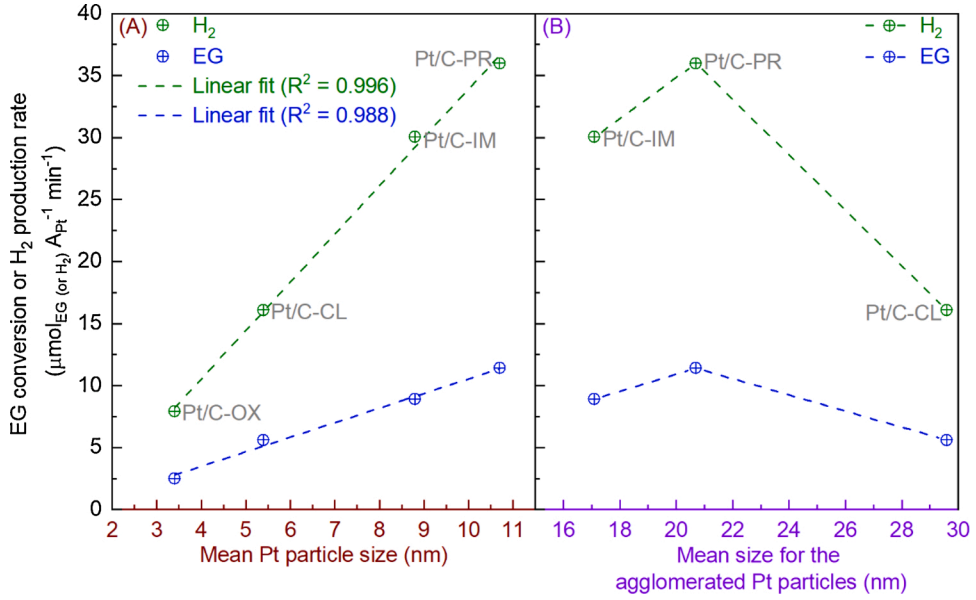

Fig. 6. Rates of EG conversion and H_2 production *versus* mean Pt particle size (A) and the size for agglomerated Pt particles (B) on various Pt/C catalysts.

exploitation of Pt/C catalyst for APR of the aqueous phase of pyrolysis oil or other waste aqueous oxygenate streams is thus recommended. On the other hand, a large amount of CO (*e.g.*, carbon yield of 18–25 %, Fig. 4B) were also formed during APR of EG over Pt/C catalysts. This indicates an inefficient water-gas shift (WGS, $CO + H_2O \rightarrow H_2 + CO_2$) reaction, in line with the low yield of CO_2 (Fig. 4B). Therefore, bio-H_2 production over Pt/C catalysts *via* APR could be further improved, *e.g.*, by adding a second metal such as Ni to enhance WGS reaction (*e.g.*, Pt-Ni/Al_2O_3 catalyst for APR of EG [43]).

4. Conclusions

Catalyst preparation protocols, including the incorporation of the metal precursor (*e.g.*, incipient wetness impregnation, precipitation, and impregnation of Pt colloid) and further treatment (*e.g.*, high-temperature calcination and reduction), affect Pt size and Pt distribution (homogeneous Pt distribution and with concentrated Pt particles on the surface).

Pt/C catalysts showed excellent H_2 yields (up to 24.1 %) for aqueous-phase reforming of ethylene glycol and excellent catalyst stabilities with a slight drop (*ca.* 4–5 %) in EG conversion (*ca.* 37.5–39.4 %) after 3.5-h TOS. The characteristics of the used catalysts after 7-h APR of EG, which were in a steady-state, were used to correlate the catalyst performance. The linear relationships between mean Pt particle size (in a range of 3–11 nm investigated) and the rates for EG conversion and H_2 production were observed.

Pt/C-PR catalyst, which was prepared by the precipitation method, had small Pt particles distributed in the catalyst as well as large Pt particles concentrated on the catalyst grain edge after TOS of 7 h. Pt/C-PR catalyst showed the highest turnover frequency for H_2 production (TOF-H_2 of 248 mol_{H2} mol_{Pt}^{-1} min^{-1}) among the four Pt/C catalysts investigated. This was attributed to the preferred Pt particles concentrated on the catalyst surface with the biggest mean Pt particle size (*ca.* 10.7 nm) and the appropriate mean size of agglomerated Pt particles (*ca.* 21 nm). This superb TOF-H_2 and the excellent stability of the Pt/C catalyst make it promising for APR of EG as compared with the state-of-the-art Pt catalysts, *viz.*, Pt/AlO(OH) (TOF-H_2 of 300 mol_{H2} mol_{Pt}^{-1} min^{-1}) and Pt/SiO_2 (TOF-H_2 of 275 mol_{H2} mol_{Pt}^{-1} min^{-1}) catalysts. Pt/C catalysts are therefore recommended for APR of other model oxygenates (*e.g.*, hydroxyacetone) present in waste streams and also APR of real waste streams (*e.g.*, the aqueous phase of pyrolysis oil) to make renewable and green H_2.

Declaration of Competing Interest

The authors declare that they have no known competing financial interests or personal relationships that could have appeared to influence the work reported in this paper.

CRediT authorship contribution statement

A.K.K. Vikla: Investigation, Conceptualization, Methodology, Validation, Writing - original draft, Writing - review & editing. **I. Simakova:** Resources, Validation, Supervision, Writing - review & editing. **Y. Demidova:** Investigation, Resources, Validation. **E.G. Keim:** Investigation, Resources, Validation, Writing - review & editing. **L. Calvo:** Investigation, Resources, Validation. **M.A. Gilarranz:** Resources, Supervision, Writing - review & editing. **Songbo He:** Conceptualization, Writing - original draft, Supervision, Writing - review & editing. **K. Seshan:** Supervision, Writing - review & editing, Funding acquisition.

Acknowledgments

The research was funded by European Union Seventh Framework Programme (FP7/2007-2013) within the project SusFuelCat under grant agreement No. 310490. Dr. Vikla would like to thank Ing. B. Geerdink for his technical and emotional support when carrying out the APR experiments, and also Ing. Benno Knaken for his expertise in maintaining the high-pressure reactors. Prof. L. Lefferts is thanked for preliminary discussions. Besides, Mrs. K. Altena-Schildkamp is thanked for BET and CO chemisorption measurements. Mr. Tom Velthuizen is thanked for XRF characterization, and Mr. Gerard Kip for XPS analysis at MESA + NanoLab. IS acknowledges with support from Ministry of Science and Higher Education of the Russian Federation.

Appendix A. Supplementary data

Supplementary material related to this article can be found, in the online version, at doi:https://doi.org/10.1016/j.apcata.2020.117963.

References

[1] K. Seshan, Chapter 9 Catalytic pyrolysis of lignocellulosic biomass, in: J. Sa (Ed.), Fuel Production With Heterogeneous Catalysis, CRC Press, Boca Raton, 2014, pp. 253–280.
[2] T.M.C. Hoang, A.K.K. Vikla, K. Seshan, Chapter 2 Aqueous-phase reforming of sugar derivatives: challenges and opportunities, in: D. Murzin, O. Simakova (Eds.), Biomass Sugars for Non-Fuel Applications, The Royal Society of Chemistry, 2016, pp. 54–88.
[3] R.R. Davda, J.W. Shabaker, G.W. Huber, R.D. Cortright, J.A. Dumesic, A review of catalytic issues and process conditions for renewable hydrogen and alkanes by aqueous-phase reforming of oxygenated hydrocarbons over supported metal catalysts, Appl. Catal. B 56 (2005) 171–186, https://doi.org/10.1016/j.apcatb.2004.04.027.
[4] R.D. Cortright, R.R. Davda, J.A. Dumesic, Hydrogen from catalytic reforming of biomass-derived hydrocarbons in liquid water, Nature 418 (2002) 964–967, https://doi.org/10.1038/nature01009.
[5] S. Dahiya, A.N. Kumar, J.S. Sravan, S. Chatterjee, O. Sarkar, S.V. Mohan, Food waste biorefinery: Sustainable strategy for circular bioeconomy, Bioresour. Technol. 248 (2018) 2–12, https://doi.org/10.1016/j.biortech.2017.07.176.
[6] I. Coronado, M. Stekrova, L.G. Moreno, M. Reinikainen, P. Simell, R. Karinen, J. Lehtonen, Aqueous-phase reforming of methanol over nickel-based catalysts for hydrogen production, Biomass Bioenergy 106 (2017) 29–37, https://doi.org/10.1016/j.biombioe.2017.08.018.
[7] G.Y. Chen, W.Q. Li, H. Chen, B.B. Yan, Progress in the aqueous-phase reforming of different biomass-derived alcohols for hydrogen production, J. Zhejiang Univ. Sci. A 16 (2015) 491–506, https://doi.org/10.1631/jzus.A1500023.
[8] M. El Doukkali, A. Iriondo, J.F. Cambra, I. Gandarias, L. Jalowiecki-Duhamel, F. Dumeignil, P.L. Arias, Deactivation study of the Pt and/or Ni-based γ-Al_2O_3 catalysts used in the aqueous phase reforming of glycerol for H_2 production, Appl. Catal. A Gen. 472 (2014) 80–91, https://doi.org/10.1016/j.apcata.2013.12.015.
[9] F. Bossola, X.I. Pereira-Hernández, C. Evangelisti, Y. Wang, V. Dal Santo, Investigation of the promoting effect of Mn on a Pt/C catalyst for the steam and aqueous phase reforming of glycerol, J. Catal. 349 (2017) 75–83, https://doi.org/10.1016/j.jcat.2017.03.002.
[10] A.S. Oliveira, J.A. Baeza, L. Calvo, N. Alonso-Morales, F. Heras, J.J. Rodriguez, M. A. Gilarranz, Production of hydrogen from brewery wastewater by aqueous phase reforming with Pt/C catalysts, Appl. Catal. B 245 (2019) 367–375, https://doi.org/10.1016/j.apcatb.2018.12.061.
[11] H.D. Kim, T.W. Kim, H.J. Park, K.E. Jeong, H.J. Chae, S.Y. Jeong, C.H. Lee, C. U. Kim, Hydrogen production via the aqueous phase reforming of ethylene glycol over platinum-supported ordered mesoporous carbon catalysts: Effect of structure and framework-configuration, Int. J. Hydrogen Energy 37 (2012) 12187–12197, https://doi.org/10.1016/j.ijhydene.2012.05.126.
[12] G. Zoppi, G. Pipitone, H. Gruber, G. Weber, A. Reichhold, R. Pirone, S. Bensaid, Aqueous phase reforming of pilot-scale Fischer-Tropsch water effluent for sustainable hydrogen production, Catal. Today (2020), https://doi.org/10.1016/j.cattod.2020.04.024.
[13] L.I. Godina, A.V. Tokarev, I.L. Simakova, P. Mäki-Arvela, E. Kortesmäki, J. Gläsel, L. Kronberg, B. Etzold, D.Y. Murzin, Aqueous-phase reforming of alcohols with three carbon atoms on carbon-supported Pt, Catal. Today 301 (2018) 78–89, https://doi.org/10.1016/j.cattod.2017.03.042.
[14] Platinum Prices and Platinum Price Charts, 2020 (accessed 8 May 2020), http://www.infomine.com/investment/metal-prices/platinum.
[15] P. Srinivasu, Highly dispersed platinum nanoparticles on mesoporous materials, Pure Appl. Chem. 82 (2010) 2111–2120, https://doi.org/10.1351/pac-con-10-03-01.
[16] J.X. Wang, J.F. Chen, Development of a simple method for the preparation of novel egg-shell type Pt catalysts using hollow silica nanostructures as supporting precursors, Mater. Res. Bull. 43 (2008) 889–896, https://doi.org/10.1016/j.materresbull.2007.05.002.
[17] A. Wawrzetz, B. Peng, A. Hrabar, A. Jentys, A.A. Lemonidou, J.A. Lercher, Towards understanding the bifunctional hydrodeoxygenation and aqueous phase reforming of glycerol, J. Catal. 269 (2010) 411–420, https://doi.org/10.1016/j.jcat.2009.11.027.

[18] M.L. Barbelli, F. Pompeo, G.F. Santori, N.N. Nichio, Pt catalyst supported on α-Al_2O_3 modified with CeO_2 and ZrO_2 for aqueous-phase-reforming of glycerol, Catal. Today 213 (2013) 58–64, https://doi.org/10.1016/j.cattod.2013.02.023.
[19] P. Mäki-Arvela, D.Y. Murzin, Effect of catalyst synthesis parameters on the metal particle size, Appl. Catal. A Gen. 451 (2013) 251–281, https://doi.org/10.1016/j.apcata.2012.10.012.
[20] J. Lemus, J. Bedia, L. Calvo, I.L. Simakova, D.Y. Murzin, B.J.M. Etzold, J. J. Rodriguez, M.A. Gilarranz, Improved synthesis and hydrothermal stability of Pt/C catalysts based on size-controlled nanoparticles, Catal. Sci. Technol. 6 (2016) 5196–5206, https://doi.org/10.1039/C6CY00403B.
[21] K. Lehnert, P. Claus, Influence of Pt particle size and support type on the aqueous-phase reforming of glycerol, Catal. Commun. 9 (2008) 2543–2546, https://doi.org/10.1016/j.catcom.2008.07.002.
[22] A.V. Kirilin, B. Hasse, A.V. Tokarev, L.M. Kustov, G.N. Baeva, G.O. Bragina, A. Y. Stakheev, A.-R. Rautio, T. Salmi, B.J.M. Etzold, J.-P. Mikkola, D.Y. Murzin, Aqueous-phase reforming of xylitol over Pt/C and Pt/TiC-CDC catalysts: catalyst characterization and catalytic performance, Catal. Sci. Technol. 4 (2014) 387–401, https://doi.org/10.1039/c3cy00636k.
[23] A. Ciftci, D.A.J.M. Ligthart, E.J.M. Hensen, Influence of Pt particle size and Re addition by catalytic reduction on aqueous phase reforming of glycerol for carbon-supported Pt(Re) catalysts, Appl. Catal. B 174–175 (2015) 126–135, https://doi.org/10.1016/j.apcatb.2015.02.027.
[24] A. Chen, P. Chen, D. Cao, H. Lou, Aqueous-phase reforming of the low-boiling fraction of bio-oil for hydrogen production: The size effect of Pt/Al_2O_3, Int. J. Hydrogen Energy 40 (2015) 14798–14805, https://doi.org/10.1016/j.ijhydene.2015.09.030.
[25] G.W. Huber, J.W. Shabaker, S.T. Evans, J.A. Dumesic, Aqueous-phase reforming of ethylene glycol over supported Pt and Pd bimetallic catalysts, Appl. Catal. B 62 (2006) 226–235, https://doi.org/10.1016/j.apcatb.2005.07.010.
[26] K. Koichumanova, A.K.K. Vikla, D.J.M. de Vlieger, K. Seshan, B.L. Mojet, L. Lefferts, Towards stable catalysts for aqueous phase conversion of ethylene glycol for renewable hydrogen, ChemSusChem 6 (2013) 1717–1723, https://doi.org/10.1002/cssc.201300445.
[27] R.R. Davda, J.W. Shabaker, G.W. Huber, R.D. Cortright, J.A. Dumesic, Aqueous-phase reforming of ethylene glycol on silica-supported metal catalysts, Appl. Catal. B 43 (2003) 13–26, https://doi.org/10.1016/S0926-3373(02)00277-1.
[28] J.W. Shabaker, G.W. Huber, R.R. Davda, R.D. Cortright, J.A. Dumesic, Aqueous-phase reforming of ethylene glycol over supported platinum catalysts, Catal. Lett. 88 (2003) 1–8, https://doi.org/10.1023/a:1023538917186.
[29] J.H. Kim, K.E. Jeong, T.W. Kim, H.J. Chae, S.Y. Jeong, C.U. Kim, K.Y. Lee, Effect of the preparation method of support on the aqueous phase reforming of ethylene glycol over 2 wt% $Pt/Ce_{0.15}Zr_{0.85}O_2$ Catalysts, J. Nanosci. Nanotechnol. 13 (2013) 5874–5878, https://doi.org/10.1166/jnn.2013.7044.
[30] J.W. Shabaker, R.R. Davda, G.W. Huber, R.D. Cortright, J.A. Dumesic, Aqueous-phase reforming of methanol and ethylene glycol over alumina-supported platinum catalysts, J. Catal. 215 (2003) 344–352, https://doi.org/10.1016/s0021-9517(03)00032-0.
[31] X.H. Liu, Y. Guo, W.J. Xu, Y.Q. Wang, X.Q. Gong, Y.L. Guo, Y. Guo, G.Z. Lu, Catalytic properties of Pt/Al_2O_3 catalysts in the aqueous-phase reforming of ethylene glycol: Effect of the alumina support, Kinet. Catal. 52 (2011) 817–822, https://doi.org/10.1134/s0023158411060115.
[32] H.D. Kim, H.J. Park, T.W. Kim, K.E. Jeong, H.J. Chae, S.Y. Jeong, C.H. Lee, C. U. Kim, Hydrogen production through the aqueous phase reforming of ethylene glycol over supported Pt-based bimetallic catalysts, Int. J. Hydrogen Energy 37 (2012) 8310–8317, https://doi.org/10.1016/j.ijhydene.2012.02.160.
[33] J.A. Baeza, L. Calvo, M.A. Gilarranz, A.F. Mohedano, J.A. Casas, J.J. Rodriguez, Catalytic behavior of size-controlled palladium nanoparticles in the hydrodechlorination of 4-chlorophenol in aqueous phase, J. Catal. 293 (2012) 85–93, https://doi.org/10.1016/j.jcat.2012.06.009.
[34] S. Brunauer, P.H. Emmett, E. Teller, Adsorption of gases in multimolecular layers, J. Am. Chem. Soc. 60 (1938) 309–319, https://doi.org/10.1021/ja01269a023.
[35] A. Le Valant, C. Comminges, F. Can, K. Thomas, M. Houalla, F. Epron, Platinum supported catalysts: predictive CO and H_2 chemisorption by a statistical cuboctahedron cluster model, J. Phys. Chem. C 120 (2016) 26374–26385, https://doi.org/10.1021/acs.jpcc.6b09241.
[36] G. Giannetto, G. Perot, M. Guisnet, Hydrocracking of n-heptane on Pt-Hzsm-5. Effect of calcination and reduction conditions, in: B. Imelik, C. Naccache, G. Coudurier, Y.B. Taarit, J.C. Vedrine (Eds.), Studies in Surface Science and Catalysis, Elsevier, 1985, pp. 265–272.
[37] J. Hagen, Industrial Catalysis: A Practical Approach, 3 ed., Wiley-VCH, Singapore, 2015.
[38] D.J.M. de Vlieger, B.L. Mojet, L. Lefferts, K. Seshan, Aqueous Phase Reforming of ethylene glycol – Role of intermediates in catalyst performance, J. Catal. 292 (2012) 239–245, https://doi.org/10.1016/j.jcat.2012.05.019.
[39] A. Ciftci, B. Peng, A. Jentys, J.A. Lercher, E.J.M. Hensen, Support effects in the aqueous phase reforming of glycerol over supported platinum catalysts, Appl. Catal. A Gen. 431-432 (2012) 113–119, https://doi.org/10.1016/j.apcata.2012.04.026.
[40] K. Koichumanova, A.K.K. Vikla, R. Cortese, F. Ferrante, K. Seshan, D. Duca, L. Lefferts, In situ ATR-IR studies in aqueous phase reforming of hydroxyacetone on Pt/ZrO_2 and Pt/AlO(OH) catalysts: The role of aldol condensation, Appl. Catal. B 232 (2018) 454–463, https://doi.org/10.1016/j.apcatb.2018.03.090.
[41] A. Takagaki, J.C. Jung, S. Hayashi, Solid Lewis acidity of boehmite gamma-AlO (OH) and its catalytic activity for transformation of sugars in water, RSC Adv. 4 (2014) 43785–43791, https://doi.org/10.1039/c4ra08061k.
[42] E. Auer, A. Freund, J. Pietsch, T. Tacke, Carbons as supports for industrial precious metal catalysts, Appl. Catal. A Gen. 173 (1998) 259–271, https://doi.org/10.1016/S0926-860X(98)00184-7.
[43] D.J.M. de Vlieger, A.G. Chakinala, L. Lefferts, S.R.A. Kersten, K. Seshan, D.W. F. Brilman, Hydrogen from ethylene glycol by supercritical water reforming using noble and base metal catalysts, Appl. Catal. B 111–112 (2012) 536–544, https://doi.org/10.1016/j.apcatb.2011.11.005.